J Biomol NMR (2013) 56:313–329
DOI 10.1007/s10858-013-9749-3

ARTICLE

^{13}C structuring shifts for the analysis of model β-hairpins and β-sheets in proteins: diagnostic shifts appear only at the cross-strand H-bonded residues

Irene Shu · Michele Scian · James M. Stewart · Brandon L. Kier · Niels H. Andersen

Received: 11 April 2013 / Accepted: 28 May 2013 / Published online: 14 July 2013

Abstract The present studies have shown that ^{13}C=O, $^{13}C^{\alpha}$ and $^{13}C^{\beta}$ of H-bonded strand residues in β-hairpins provide additional probes for quantitating the extent of folding in β-hairpins and other β-sheet models. Large differences in the structuring shifts (*CSD*s) of these ^{13}C sites in H-bonded versus non-H-bonded sites are observed: the differences between H-bonded and non-H-bonded sites are greater than 1.2 ppm for all three ^{13}C probes. This prompts us to suggest that efforts to determine the extent of hairpin folding from ^{13}C shifts should be based exclusively on the observation at the cross-strand H-bonded sites. Furthermore, the statistics suggest the $^{13}C'$ and $^{13}C^{\beta}$ *CSD*s will provide the best differentiation with 100 %-folded *CSD* values approaching −2.6 and +3 ppm, respectively, for the H-bonded sites. These conclusions can be extended to edge-strands of protein β-sheets. Our survey of reported ^{13}C shifts in β-proteins indicates that some of the currently employed random coil values need to be adjusted, particularly for ionization-induced effects.

Keywords β-hairpin · β-sheet · ^{13}C chemical shift deviations · Folding probes · ^{13}C statistical coil shifts

Electronic supplementary material The online version of this article (doi:10.1007/s10858-013-9749-3) contains supplementary material, which is available to authorized users.

I. Shu · M. Scian · J. M. Stewart · B. L. Kier · N. H. Andersen (✉)
Department of Chemistry, University of Washington, Seattle, WA 98195, USA
e-mail: andersen@chem.washington.edu

Introduction

It has long been recognized that ^{13}C=O, $^{13}C^{\alpha}$ and $^{13}C^{\beta}$ chemical shift deviations (*CSD*s) from random coil values strongly correlate with protein backbone conformations (Spera and Bax 1991; Wishart et al. 1991) and ^{13}C *CSD*s have been incorporated into schemes for assigning protein secondary structure (Wishart and Sykes 1994). By cross-correlating X-ray crystallography structures with NMR chemical shifts, it was found that $^{13}C^{\alpha}$ and carbonyl shifts are downfield relative to random coil norms within helices and upfield within β-structures, whereas $^{13}C^{\beta}$ shifts display the opposite trend (Spera and Bax 1991). Although the range of ^{13}C *CSD*s occurring in β-sheets slightly overlaps with the narrower range for α-helices, ^{13}C chemical shifts can be very useful for assigning secondary structure and thereby determining the 3D structure of a protein (Wishart and Sykes 1994; Avbelj et al. 2004). In 2008 Vila and Scheraga (Vila et al. 2008; Vila and Scheraga 2008) classified nuclei in proteins in order of the usefulness of their *CSD*s in elucidating secondary structure; for β-structure definition the following sequence was given: $^{1}H^{\alpha} > {}^{13}C^{\beta} > {}^{1}H^{N} \sim {}^{13}C^{\alpha} \sim {}^{13}C{=}O \sim {}^{15}N$. Given the larger secondary structure shifts associated with ^{13}C nuclei, this statistical observation was somewhat surprising.

For β-structures, an i/i + 2 periodicity in $^{1}H^{\alpha}$ structuring shifts, with the cross-strand directed $^{1}H^{\alpha}$'s of non-H-bonded hairpin sites further downfield than those of H-bonded sites, was recognized quite early in studies of designed hairpins (Andersen et al. 1999, 2002, 2004; Griffiths-Jones et al. 1999; Tatko and Waters 2003; Fesinmeyer et al. 2004) and subsequently it was established that this also applies to protein β-sheets (Sharman et al. 2001; Fesinmeyer et al. 2005a). A similar trend for $^{1}H^{N}$ along hairpin strands, with the downfield chemical shift

deviations (*CSD*s) appearing at H-bonded sites, only became apparent in studies of hairpin models (Andersen et al. 2004), although they also could be confirmed in β-protein shift data (Fesinmeyer et al. 2005a). We employed the *CSD*s of the further downfield $^{1}H^{\alpha}$ and $^{1}H^{N}$ sites for hairpin fold quantitation as early as 1999 (Andersen et al. 1999) and have recommended them as an alternative to assuming a 0.40 ppm average downfield shift of hairpin strand $^{1}H^{\alpha}$'s (Santiveri et al. 2001) as a basis for fold population estimation. The Madrid group (Santiveri et al. 2001, 2005) has also provided guidelines for using $^{13}C^{\beta}$ and $^{13}C^{\alpha}$ *CSD*s for hairpin fold stability estimation (based on +1.95 and −1.55 ppm shifts, respectively, averaging over all non-terminal strand sites). The present study was undertaken to determine whether site specific (non-H-bonded vs H-bonded) analysis of ^{13}C strand shifts could improve such analyses. With the exception of our preliminary report (Shu et al. 2011) of a portion of this data, differential ^{13}C shift diagnostics of such sites do not appear to have been recognized in literature to date.

There have also been reports concerning the sources of chemical shift differentiation upon peptide or protein folding. Full ab initio computational studies showed that ϕ, ψ torsion angles dominate the shielding of the ^{13}C nuclei (de Dios et al. 1993; Xu and Case 2002) and this conclusion has been supported by experimental data for proteins (Iwadate et al. 1999). Factors such as backbone hydrogen bonding and electrostatic interactions also influence the shielding effect. They were considered to make the calculated carbon chemical shifts correlate better with the measured values (de Dios et al. 1993; de Dios and Oldfield 1994), even though the examination using Density Function Theory (DFT) suggested that they contribute at most 1 ppm to structuring shifts in hairpin and β-sheet structures (Xu and Case 2002). Differential solvent exposure is another feature with an established influence on chemical shifts (Avbelj et al. 2004). Thus, there were reasons to expect differentiation in the ^{13}C shifts of strand positions in an isolated β-hairpin; the strand residues are alternately cross-strand hydrogen bonded or solvent exposed (non-hydrogen bonded).

The present study indicates that the diagnostic ^{13}C=O, $^{13}C^{\alpha}$ and $^{13}C^{\beta}$ *CSD*s for β-structuring are associated, almost exclusively, with the cross-strand hydrogen-bonded residues. We have provided (Shu et al. 2011) a partial rationale for this observation. These structuring shift magnitudes, particularly the ^{13}C=O and $^{13}C^{\beta}$ *CSD*s, provide quantitative correlations with hairpin fold populations. The present study also indicates that backbone ^{13}C shifts, even for the statistical coil state, are strongly solvent dependent. Fluoroalcohol addition, which often improves hairpin stability (Andersen et al. 1999), induces quite large shifts (as much as 2.2 ppm) for backbone $^{13}C^{\beta}$ sites in non-folded controls; these need to be taken into account in hairpin structure analysis and quantitation. Also, contrary to earlier expectations (Iwadate et al. 1999; Santiveri et al. 2001), ring current shifts can, in some cases, be as large as secondary structure shifts for $^{13}C^{\alpha}$ and $^{13}C^{\beta}$ sites.

Methods and materials

Peptide models: selection and synthesis

Twenty-six peptides were examined in the present study. Many were ^{13}C=O isotopomers of previous constructs, but seven were new constructs that are analogs of prior series. In all cases, the peptide series have been thoroughly characterized by NMR and CD studies (Fesinmeyer et al. 2005a; Andersen et al. 2006; Kier and Andersen 2008; Kier et al. 2010; Eidenschink et al. 2009a, b). A wide variety of hairpin fold stabilities are included as a result of both strand and turn mutations in the MrH peptide series (Maynard et al. 1998; Fesinmeyer et al. 2005a; Eidenschink et al. 2009b); in addition, species stabilized by a Ac–W—WTG capping motif (Kier and Andersen 2008; Kier et al. 2010), and a three-stranded sheet analogous to the constructs first reported from the Gellman laboratory (Schenck and Gellman 1998; Fesinmeyer et al. 2005a; Hudson and Andersen 2006), and a "turnless" sheet held together by a disulfide linkage was included in order to explore a greater variety of strand lengths and structural complexity. Unstructured coil reference peptides, including species with a higher proportion of β-branched residues that might be expected to prefer extended-strand configurations, were constructed with and without $^{13}C'$ labels at valine and alanine. These peptides and controls appear in Table 1. Aromatic-residue containing peptides (Eidenschink et al. 2009a, b; Huggins and Andersen 2010) were included to probe ring-current effects on ^{13}C structuring shifts.

All peptide hairpins were synthesized on an Applied Biosystem 433A peptide synthesizer using standard Fmoc solid-phase peptide synthesis methods. Wang resins preloaded with the C-terminal amino acid were employed. C-terminal amides were prepared similarly but using Rink resins. $^{13}C'$-labeled valine and alanine were converted to their Fmoc derivative using Fmoc-OSu (N-fluorenylmethyl succinimidyl carbonate) in acetone–water mixtures containing $NaHCO_3$ (16 h with stirring). N-terminal acetylation was performed by adding the peptide bound resin to a 3 mL DMF (N,N-dimethylformamide)/95 μL acetic anhydride/140 μL triethylamine mixture and shaking for 1 h. Peptides are cleaved from the resin using a 95:2.5:2.5 trifluoroacetic acid (TFA): tri-isopropylsilane: water mixture. The cleaved peptides were purified by reverse phase HPLC

Table 1 Peptides examined

MrH hairpins	
MrH3b	KKYTVS-IpGK-KITVSA
MrH3b-VTS	KKYVTS-IpGK-KIVTSA
Ac-MrH3d	Ac-KKYTVS-IPGK-KITVSA
MrH3d	KKYTVS-IPGK-KITVSA
MrH4a	KKLTVS-INGK-KITVSA
MrH4a-T13A	KKLTVS-INGK-KIAVSA
MrH4b	KKLTVS-IpGK-KITVSA
MrH4e	KKLTVS-IUGK-KITVSA
MrH5b	KKYTVS-IpGK-KVTVSA
MrH5b+2	KKYTVS-IpGK-KVTVSA
MrH6e	KKLTVS-IUGK-KIVTSA
MrH4f	KKLTVS-IpPK-KIZVSA
β-capped hairpins	
βcap2-INGK	Ac-W--INGK-WTG-NH_2
βcap4-NPDGK	Ac-WVS-NPDGK-KIWTG-NH_2
βcap6-NG(A3)	Ac-WIAVT--INGK-KIRVWTG-NH_2
βcap6-(−W1)	Ac- IAVT--INGK-KIRVWTG-NH_2
βcap6-HG	Ac-WITVT--IHGK-KIRVWTG-NH_2
βcap6-HG(A4)	Ac-WITAT--IHGK-KIRVWTG-NH_2
[4:6] hairpin class	
HP7-(Z=T/A)	KZW-NPATGK-WZE
HP7T-NAAAGK	KTW-NAAAGK-WTE
Other sheet models	
EPDGK-pG	Ac-VFIT-EPDGK-TYTE--VpGO-KILQ-NH_2
turnless-C_2	KWRTIKVCITKRTWE disulfide
Random coil controls	
RCA	Ac-GKAAAK-NH_2
βRCA	Ac-KIAVSAK-NH_2
βRCV	Ac-KITVSAK-NH_2
RCV	Ac-GKAVAAK-NH_2
MrH2	Ac-GKKITVSA
RCV2	Ac-KAAVAA
CRS-E	Ac-RKAEAGS
Peptides for aromatic-effect study	
HP6Va3	KAVYI-NG-KWTVE
MrH4bW2	KKLTVWI-pG-KWITVSA
MrH4bW3	KKLTWSI-pG-KKWTVSA
MrH4bW4	KKLWVSI-pG-KKIWVSA
MrH4W(±4)-XG	KKLWVSI-XG-KKIWVSA
MrH4W(-4)-NG	KKLWVSI-NG-KKIAVSA

p = D-Pro, U = Aib, O = ornithine, **X** is used for $^{13}C'$-isotopic forms of amino acid residues. **Z** is used for a site that was examined as T and A or **A**, **XG** corresponds to both NG and AG

on a Varian C18 prep-scale column using gradients of water/acetonitrile (having 0.1 and 0.085 % TFA respectively). Collected fractions were lyophilized and their identity and molecular weight confirmed using a Bruker Esquire Ion Trap mass spectrometer. Sequence and purity were verified by ^{1}H NMR.

NMR data collection

All NMR samples included 10 % D_2O and were prepared at 0.5–2 mM peptide concentration in 50 mM, pH 6.0 potassium phosphate buffer, except for the three-stranded sheet EPDGK-pG that was studied in 20 mM, pH 3.0 buffer. DSS (2,2-dimethyl-2-silapentane-5-sulfonate) and/or ^{13}C urea served as internal reference standards. Deuterated hexafluoroisopropanol (HFIP) or β-trifluoroethanol (TFE) was added to the vol% as noted; the aqueous portion was added by pipette with the volatile fluoroalcohol delivered by glass microliter syringes. For natural abundance ^{13}C experiments, the samples were prepared using D_2O buffers.

The $^{13}C'$ chemical shifts of isotopically labeled valine and alanine residues were obtained from 1D ^{13}C experiment on a Bruker AV500 instrument at 125.72 MHz with a 30 ppm spectral width (32 K points), centered at 169 ppm, and 64–512 scans depending on sample concentration and signal to noise. ^{13}C-urea served as the internal shift reference as previously described (Fesinmeyer et al. 2005b). The chemical shifts of ^{13}C-urea, versus DSS, for the media used in this study are tabulated in the Supplementary Material. For aqueous medium without co-solvent addition, the ^{13}C-urea shift (in ppm) is given by $\delta = 165.609 - 0.0056 \times T$ (T = °C).

$^{13}C^{\alpha}$ and $^{13}C^{\beta}$ chemical shifts of all residues were measured by a natural abundance 2D ^1H-^{13}C HSQC experiment (Vuister and Bax 1992) on a Bruker DRX instrument ($^1H/^{13}C$ 499.85/125.69 MHz), spectral width 10/85 ppm, center frequency at 3.80/37.00 ppm, with 1,024/256 time domain points and 80 scans per time point. ^{13}C nuclei were assigned by the cross peaks associated with the covalently bonded ^1H frequencies based on previously reported data or proton assignments through a combination of 2D ^1H-^1H TOCSY and NOESY experiments with WATERGATE (Piotto et al. 1992) solvent suppression. TOCSY employed a 80 ms MLEV-17 spinlock (Bax and Davis 1985) and NOESY a 150 ms mixing time for 8 and 16 scans, respectively.

Residue nomenclature for β-hairpins

For the convenience of description throughout the paper, a β-hairpin nomenclature is presented in Fig. 1.

T indicates turn positions (which can be from 2 to 4 in number), and S indicates strand positions numbered from the turn locus. S ± even-numbered positions are non-H-bonded and have their H^{α}'s directed inward; S ± odd-numbered strand positions (with the exception of S − 1) are designated as H-bonded sites. An (S − 1, T1, T2, S + 1)-β-turn sequence is often described as the *i*, *i* + *1*, *i* + *2* and *i* + *3* positions of a four residue turn in a [2:2] or

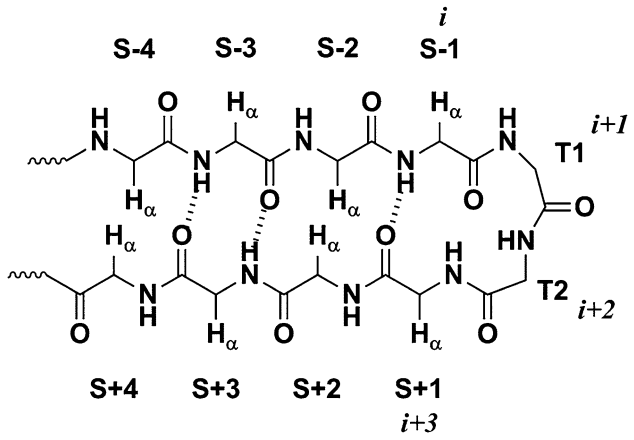

Fig. 1 β-Hairpin nomenclature

[2:4]-hairpin (Sibanda and Thornton 1991). T1, T2, T3 are employed for [3:5]-hairpin turns (EPDGK and NPDGK in the present study); the T1, T2, T3, T4 sites in a [4:6]-hairpin are underlined: NPATGK. This nomenclature maintains the S ± odd/S ± even designations for H-bonded versus non-bonded sites remote from the turn. The S + 1 sites also have an H-bonded carbonyl and are included in the HB category. The S − 1 site is H-bonded in some tight turns as well as in [3:5]- and [4:6]-hairpins; these sites are designated as "turn H-bonded" sites herein.

Hairpin fold population determination

Previously published proton random coil values and near-neighbor sequence corrections (Fesinmeyer et al. 2004; Eidenschink et al. 2009b) are used throughout to determine $^{1}H^{\alpha}$ and $^{1}H^{N}$ *CSD*s ($\delta_{obs} - \delta_{random\ coil}$). Diagnostic 100 %-folded ^{1}H *CSD* reference values have been established (Eidenschink et al. 2009b; Kier and Andersen 2008, 2009; Hudson and Andersen 2006) for the MrH, β-cap and three-stranded sheet scaffolds employed herein. The diagnostic sites employed are cross-strand directed $^{1}H^{\alpha}$'s, $^{1}H^{N}$'s (Fesinmeyer et al. 2005a), and protons with larger shifts (>1 ppm) due to ring current effects. Fold population (fraction folded, χ_F) is thus determined as $CSD_{obs}/CSD_{100\ \%}$ from each of the diagnostic protons and averaged. In the case of the β-cap hairpins, the 100 % folded *CSD*s have been verified by backbone amide exchange protection factors; there are representatives of these folds with $\chi_F > 0.97$ based on the exchange protection factors (Kier and Andersen 2008; Kier et al. 2010).

^{13}C CSD calculations

There are two major compilations of experimental ^{13}C random coil shift values: (1) chemical shifts determined by Wishart et al. (1995) using Ac-GGXAGG-NH_2 and Ac-GGXPGG-NH_2 peptide models provide one basis and the specific measure of the Pro effect on the preceding residue, and (2) chemical shifts along with sequence-dependent correction determined by Schwarzinger et al. (2000, 2001) using Ac-GGXGG-NH_2 model peptides. The sequence corrections of Schwarzinger, based on changes in the glycine shifts in the model peptides have, in the case of ^{1}H shifts, been shown to be specific to the "all glycines" context; different near-neighbor corrections have been observed for -AAXAA- contexts (Eidenschink et al. 2009b; Fesinmeyer et al. 2004). In the case of our $^{13}C'$ reference peptides (Table 1), the "apparent *CSD*" calculated using the Schwarzinger coil shifts was −0.42 ± 0.13 ppm. For $^{13}C^{\alpha/\beta}$ shifts, "apparent *CSD*s" as large as 0.6 and 1.3 ppm result for our coil reference peptides. With the Wishart values, these differences for $^{13}C^{\alpha/\beta}$ shifts were all <0.2 ppm.

Solvent induced changes in $^{13}C'$ shifts were context dependent and quite large, as large as the β-structuring shifts in some cases (see Table 2). As a result, we used direct differencing between observed shifts for hairpin models using the most similar controls at the matching solvent conditions and temperature to derive our $^{13}C'$ *CSD*s.

The HFIP addition effect on $^{13}C^{\alpha}$ and $^{13}C^{\beta}$ shifts was minimal at 8 vol%, in the same direction as observed for $^{13}C'$ for 20 vol% HFIP; but TFE addition had opposite effects on carbonyl and non-carbonyl sites. Based on this data (Table 2), all $^{13}C^{\alpha/\beta}$ random coil shifts were adjusted by +0.9 ppm prior to calculating *CSD*s for peptides in 20 % HFIP (see Fig. 4, vide infra).

In the case of $^{13}C^{\alpha}$ and $^{13}C^{\beta}$ shifts we examined, in addition to experimental values of Wishart and Schwarzinger, the average values for each residue in the BMRB (Biological Magnetic Resonance data Bank) database (http://www.bmrb.wisc.edu/ref_info/statsel.htm), as an alternative value for δ_{ref} : $CSD_{BMRB} = \delta_{obs} - \delta_{ref}$. A comparison of the three referencing methods appears as Fig. S1 (Supplementary Material). On that basis, we selected the Wishart random coil values, with a near-neighbor correction only for a following Pro, for the calculation of all the $^{13}C^{\alpha/\beta}$ *CSD*s reported herein.

However, with the Wishart coil values measured at pH 5, ionization-induced changes need to be considered. Effects of sidechain carboxylate protonation were evident in a comparison of Wishart and Schwarzinger (pH 2.3, 8 M urea) coil values. In the case of non-ionizable sidechains, the Schwarzinger $^{13}C^{\beta}$ shifts are 0.13 ± 0.08 ppm downfield; in the case of Asp, a 2.8 ppm upfield shift was observed for protonation. Similar comparisons for $^{13}C^{\alpha}$ shifts were: neutral sidechains (+0.33 ± 0.20), Glu (−0.5), and Asp (−1.2 ppm). To directly measure C-terminal

Table 2 Solvent effects on ^{13}C shifts referenced to DSS at 280 K

	Δδ (co-solvent), ppm		
	8 % HFIP	20 % HFIP	30 % TFE
^{13}C-Urea	+0.45	+1.05	−2.33
$^{13}C = O$ shifts			
KAAAK	+0.26	+1.41	−2.34
KIAVS	+0.21	+1.58	−2.62
GKAVAA	+0.26		
KAVAA	+0.16	+1.03	−2.64
KTVSK	+0.22		
KIVTS	+0.26	+1.16	
Averages	+0.23 ± 0.04	+1.30 ± 0.26	−2.53 ± 0.17
$^{13}C^{\alpha}/^{13}C^{\beta}$ shifts			
RCV2			
K1	+0.00/0.14	+0.97/0.97	+0.50/0.71
A2	+0.04/0.05	+0.97/0.81	+0.54/0.53
A3	+0.04/0.05	+1.02/1.00	+0.54/0.53
V4	−0.01/+ 0.14	+0.85/0.81	+0.38/0.75
A5	+0.04/0.05	+0.81/0.86	+0.54/0.53
A6	+0.01/0.05	+0.84/0.88	+0.32/0.56
MrH2			
G1		+0.91/	+0.55/
K2		+0.99/0.90	+0.61/0.68
K3		+0.99/0.90	+0.61/0.67
I4		+1.16/0.94	+0.81/0.69
T5		+0.66/0.87	+0.26/0.64
V6		+0.93/0.80	+0.59/0.56
S7		+0.65/1.01	+0.33/0.71
A8		+0.81/0.74	+0.47/0.53
Averages	+0.02 ± 0.02/0.08 ± 0.05	+0.90 ± 0.14/0.88 ± 0.08	+0.50 ± 0.14/0.62 ± 0.08

ionization effects, we determined the pH dependence of *CSD*s of the C-terminal alanines of RCV2 (A6) and MrH2 (A8): A6 ($^{13}C^{\alpha}/^{13}C^{\beta}$) +1.28/+1.01 at pH 6.8, −0.46/+0.05 at pH 3, A8 ($^{13}C^{\alpha}/^{13}C^{\beta}$) +1.48/+1.01 ppm at pH 6.8. We also determined the pH titration effects for the Glu and terminal Ser of CRS-E. Based on these results we employ the following corrections to Wishart coil values (Δrc, in ppm): C-terminal AA–CO_2^- (+1.45 for $^{13}C^{\alpha}$, +1.0 for $^{13}C^{\beta}$), C-terminal AA–CO_2H (−0.45 for $^{13}C^{\alpha}$, +0.1 for $^{13}C^{\beta}$), Glu^- (+0.4 for $^{13}C'$, −0.36 for $^{13}C^{\alpha}$, +0.4 for $^{13}C^{\beta}$), Glu^0 (−1.0 for $^{13}C^{\alpha}$, −1.0 for $^{13}C^{\beta}$), Asp^- (+0.9 for $^{13}C'$, +0.2 for $^{13}C^{\alpha}$, +0.4 for $^{13}C^{\beta}$) and Asp^0 (−1.0 for $^{13}C^{\alpha}$, −2.4 ppm for $^{13}C^{\beta}$).

Structural data mining from the ^{13}C chemical shifts of protein β hairpins in BMRB database

Residues in hairpin and sheets are classified into three categories based on their H-bonding state: "Edge H-bonded" ("Inny" in Fig. 2), a residue on an edge-β-strand which is H-bonded with the neighboring strand; "Central" residues are H-bonded to two neighboring strands; and "Non-H-bonded" ("Outy") residues which are on an edge-β strand and are not H-bonded to either the adjacent β-strand or with any other site. These criteria were filtered by the BMRB_Parse Program which downloads the corresponding PDB files, runs the PDB files through STRIDE to search for hairpins, and cross checks those hairpins with BMRB data in order to obtain ^{13}C shifts and H-bonding status for all applicable residues. *CSD*s were calculated using Schwarzinger random coil values including the published (2001) near-neighbor corrections for these values. The *CSD*s were binned in 0.25 ppm intervals and the resulting histogram for each H-bonding class was fitted to a Gaussian; both the centers of the Gaussians, as well as their σ values, and global means for each category were reported by the program. The ^{13}C=O analysis was performed with data through 1/2009 returning 7 k *CSD*s;

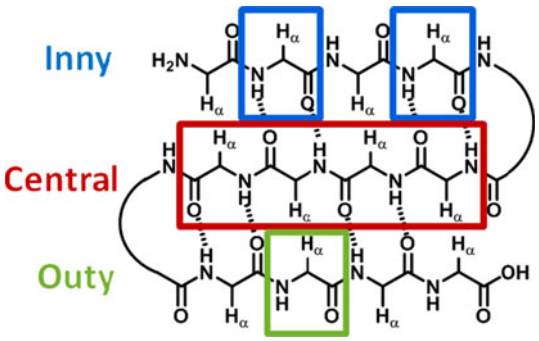

Fig. 2 The three categories of residues in a β-sheet

the resulting *CSD* values were then averaged for each of the three categories. The number of useful instances for residues ranged from 128 (for Trp) to 977 (for Val). The fraction of occurrences that corresponded to non-H-bonded sites was 0.311 ± 0.051 over all residues except Gly, His, and Pro. These three residues had too few occurrences in one or another of the categories and were excluded in the case of the $^{13}C=O$ data statistics. The $^{13}C^{\alpha}/^{13}C^{\beta}$ analysis was performed in 3/2013 and returned 19 k $^{13}C^{\beta}$ and 28 k $^{13}C^{\alpha}$ *CSD*s.

Results

We inserted a variety of turns and mutations into the well-studied MrH hairpin scaffold (Maynard et al. 1998; Andersen et al. 1999; Fesinmeyer et al. 2005a; Eidenschink et al. 2009b) providing systems with a wide range of fold populations to examine how the extent of folding affects $^{13}C=O$, $^{13}C^{\alpha}$ and $^{13}C^{\beta}$ chemical shifts. The study was also extended to hairpins with different turn types and a three-stranded sheet (double hairpin) motif. We expected to observe an alternating magnitude pattern in ^{13}C *CSD*s histograms of the designed hairpins with the *CSD* magnitudes reflecting the fold population. The $^{13}C=O$ data, where a differentiation between cross-strand hydrogen bonded versus solvent exposed sites was expected, will be presented first. Throughout, the H-bonded residues in hairpins will be indicated by bold underlined residue symbols.

$^{13}C=O$ *CSD*s along β-strands

Two Val $^{13}C=O$ labels were incorporated into each MrH hairpin, one on each β-strand, selectively at cross-strand hydrogen bonded and non-hydrogen bonded positions as shown in Table 1. All fraction folded values (χ_F) were derived from $^{1}H^{\alpha}$ and $^{1}H^{N}$ *CSD*s as previously described (Eidenschink et al. 2009b). In the essentially random coil construct (Ac-MrH3d, with an L-Pro-Gly "turn locus"),

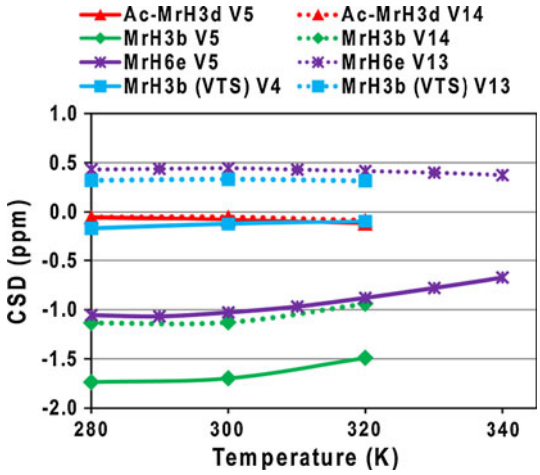

Fig. 3 $^{13}C=O$ *CSD* melting *curves* of the N-terminal and C-terminal Val residues of MrH hairpin models in aqueous medium at pH 6

both $^{13}C'$ showed no *CSD*s versus the sequence-matched reference peptide, βRCV (Fig. 3).

Figure 3 also includes a construct with both $^{13}C=O$ cross-strand H-bonded (MrH3b, $\chi_F = 0.60$ at 280 K), one with only the N-terminal site H-bonded (MrH6e, $\chi_F = 0.47$ at 280 K), and one with both carbonyls outwardly directed (MrH3b-VTS, $\chi_F = 0.32$ at 280 K). Only the intramolecularly H-bonded carbonyls display significant structuring shifts, uniformly in upfield direction. The H-bonded sites were also the only ones displaying a *CSD* magnitude melt as the fold population decreases on warming. The observation of structuring shifts at the H-bonded sites was expected, but the direction of the shift was unanticipated and has only been rationalized recently (Shu et al. 2011).

A few other hairpin constructs served to establish that these features were not specific to the MrH scaffold. The notable effect of hairpin fold stabilization by the introduction of a terminal β-capping unit (Kier et al. 2010) serves as an illustration. Peptide Ac-I**A**V**T**-INGK-KIR-VWTG-NH_2, which lack the N-terminal Trp required for a β-capping interaction, displays ^{1}H *CSD*s indicating a hairpin fold population ≤0.11 and has $^{13}C'$ *CSD*s of −0.22 and +0.16 ppm, respectively for the labeled alanine and valine. Upon capping (insertion of the N-terminal Trp affording βcap6-NG(A), Ac-W**I**A**V**T-INGK-K**I**R**V**WTG-NH_2), the ^{1}H *CSD*s indicate $\chi_F = 0.71$ and the $^{13}C'$ *CSD*s change to −0.47 and −1.55 ppm: reflecting a 1.7 ppm upfield shift for the H-bonded valine site. In a more stable capped construct, Ac-W**I**T**A**T-IHGK-K**I**R**V**WTG-NH_2 ($\chi_F = 0.90$, βcap6-HG(A) in Table S2), 100 %-folded the *CSD*s increase to −2.23 and −2.14 ppm, respectively, for the H-bonded Ala and Val. It appears that large upfield shifts of $^{13}C'$ are, indeed, associated with the H-bonded β-strand sites of hairpins and that the shifts approach 2.6 ppm for fully folded species. A complete analysis (Shu et al.

2011) of the ^{13}C=O shifts in Table S2 has revealed a linear correlation between H-bonded $^{13}C'$ *CSD*s and fold population. As a result, we view the $^{13}C'$ *CSD*s of H-bonded strand sites in hairpins as an excellent probe for assessing both fold populations and melting characteristics.

The pattern of $^{13}C^{\alpha}$ and $^{13}C^{\beta}$ *CSD*s along β-strands and their correlation with the extent of hairpin formation (% fold)

Since we anticipated that aromatic ring current shifts could influence these *CSD*s, we chose peptide models without aromatic sidechains for our initial $^{13}C^{\alpha/\beta}$ studies. The first requirement for the use of $^{13}C^{\alpha/\beta}$ shifts as structural and melting probes was defining suitable statistical coil reference shifts. We evaluated three potential sources of reference shifts: average chemical shift entries in Biological Magnetic Resonance data Bank (BMRB), random coil values and neighboring effect adjustments due to Schwarzinger et al. (2000, 2001) and the measured values for reference peptides published by Wishart et al. (1995). $^{13}C^{\alpha/\beta}$ *CSD* histograms, calculated using each set of reference values, along the sequences of numerous hairpins were examined; the comparisons for peptide MrH4b appear in Fig. S1 (Supplementary Material). The failure of BMRB-referencing for sites preceding a Pro, which has a 2.0(±0.2) and 0.5(±0.3) ppm upfield effect on $^{13}C^{\alpha}$ and $^{13}C^{\beta}$, respectively based on Wishart's studies, was immediately evident. Also, as universal averages, the BMRB reference values likely reflect the relative occurrence statistics (β vs α) of different residues. With or without the near neighbor correction, the Schwartzinger coil values gave *CSD*s that did correlate as well with ^{1}H *CSD* measures of folding as the Wishart-based *CSD*s.

For a more quantitative examination, the partially folded MrH4a system was selected so that we could increase the hairpin fold population ($\chi_F = 0.29$ in water) by both fluoroalcohol addition ($\chi_F = 0.84$ in 20 % HFIP at 300 K) and an NG → **p**G turn mutation (MrH4b, $\chi_F = 0.57$ in water, $\chi_F \approx 0.95$ in 20 % HFIP at 300 K). The observed $^{13}C^{\alpha}$ and $^{13}C^{\beta}$ *CSD*s, calculated using the Wishart et al. (1995) random values, appear in panel a) of Fig. 4.

For both MrH4a and MrH4b in aqueous solution, alternating magnitudes of the *CSD*s are clearly evident; however this pattern is only seen in 20 % HFIP data after including a solvent correction into the *CSD* calculation (Fig. 4, panel b). The correlation with previously determined χ_F-values was particularly good for the $^{13}C^{\beta}$ *CSD*s. As detailed in the Methods section, a uniform +0.90 ppm correction in random coils shifts is required for 20 % HFIP. Without this correction, the $^{13}C^{\alpha}$ *CSD*s imply that HFIP decreases the fold population. With this correction, the relative magnitudes of both ^{13}C *CSD*s reflect the established χ_F values, including the magnitude of the incremental χ_F increase associated with HFIP addition. The opposite sign $^{13}C^{\alpha/\beta}$ shifts at X in the XG loci presumably reflect the more helix-like ϕ/ψ values in the reversing turn.

Despite ring current shifts at some sites (vide infra), analogs of MrH4 with a cross-strand pair of Trp residues at the S ± 4 positions provide another examples of the excellent correlation between ^{1}H and ^{13}C *CSD* measures of folding. It has previously been established that Trp residues have a higher β-propensity than Thr and favorable cross-strand interactions at some positions. However, in the case of the S ± 4 pairing, there does not appear to be a favorable cross-strand indole/indole interaction geometry: the Trp residues do not display restricted side chain conformations. The enhanced β-propensity does impart greater tolerance of turn mutations. Based on prior studies (Eidenschink et al. 2009b), for MrH4W4, a **p**G → AG mutation is destabilizing by only 2.0 kJ/mol. This fold population change is evident in all panels of Fig. 5: the decreased *CSD*s at the H-bonded amide $^{1}H^{N}$ sites and in the cross-strand directed $^{1}H^{\alpha}$'s in the N-terminal strand (panel a) were the basis for the original $\Delta\Delta G_U$ estimate. Even though some of the ^{1}H and ^{13}C sites have ring current shifts, it appears that all of the ^{13}C *CSD*s (panel b) display a similar loss in magnitude due to the fold destabilizing **p**G → AG mutation. With the inclusion of ^{13}C shift melt data and the mutational data, the case for a two-state folding scenario for these hairpins and other similar hairpins (see Fig. S2) is strengthened. The larger changes in ^{13}C *CSD*s in the IXGK turn (Fig. 5) may reflect either turn geometry changes or that this reversing loop displays greater segmental motion in the case of IAGK.

The four $^{13}C^{\beta}$ *CSD*s of the H-bonded sites surrounding the non-H-bonded W/W pair appear to provide the most accurate reflection of the change in fold population at any particular temperature. However, when *CSD* melts were examined, the decreases in $^{13}C^{\beta}$ *CSD*s were typically larger than those observed for the $^{1}H^{\alpha}$ and $^{13}C^{\alpha}$ *CSD*s, an example of this effect appears in Fig. S2. The differentiation of $^{13}C^{\alpha}$ and $^{13}C^{\beta}$ melting profiles can most readily be seen in a peptide that display cold-denaturation (Andersen et al. 1999; Dyer et al. 2004, 2005; Fesinmeyer et al. 2005a; Andersen et al. 1996) with maximal fold stability at 300 K rather than at the low temperature limit. The melting profiles for MrH4W(±4)-AG appear in Fig. 6.

In Fig. 6, the $^{13}C^{\alpha}$ shift melts mirror the fold fractions determined by ^{1}H shift and CD melts (data not shown). In contrast, the $^{13}C^{\beta}$ *CSD*s indicate steady melting throughout the temperature range examined rather than maximal folding at the intermediate temperature. One explanation for this would be an increased randomization of the sidechain rotamer preferences at the H-bonded strand sites on warming and that there is a different sensitivity of $^{13}C^{\alpha}$ versus $^{13}C^{\beta}$ shifts to sidechain torsional angles (χ_1). However, differences in sidechain

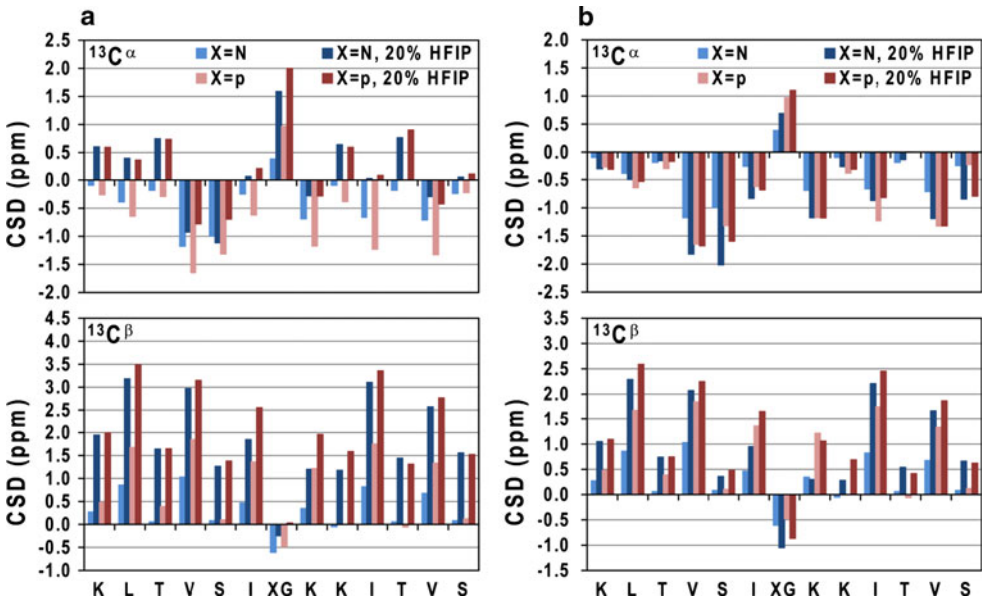

Fig. 4 *CSD* histograms at 300 K for MrH4a and MrH4b in aqueous (*lighter colored*) and 20 % HFIP solution (*darker colored*). The terminal residues were excluded and only the *CSD*s of the X residue of the XG turn loci are included here and in subsequent figures. **a** All the $^{13}C^{\alpha/\beta}$ *CSD*s were calculated based on the Wishart's random coil reference values (Wishart et al. 1995). Similar plots using alternative reference values appear in the Supplementary Material. In **b**, the *CSD*s for 20 % HFIP employed random coil reference values uniformly increased by 0.9 ppm; with this adjustment, the histograms reflect the established increase in hairpin fold population associated with fluoroalcohol addition

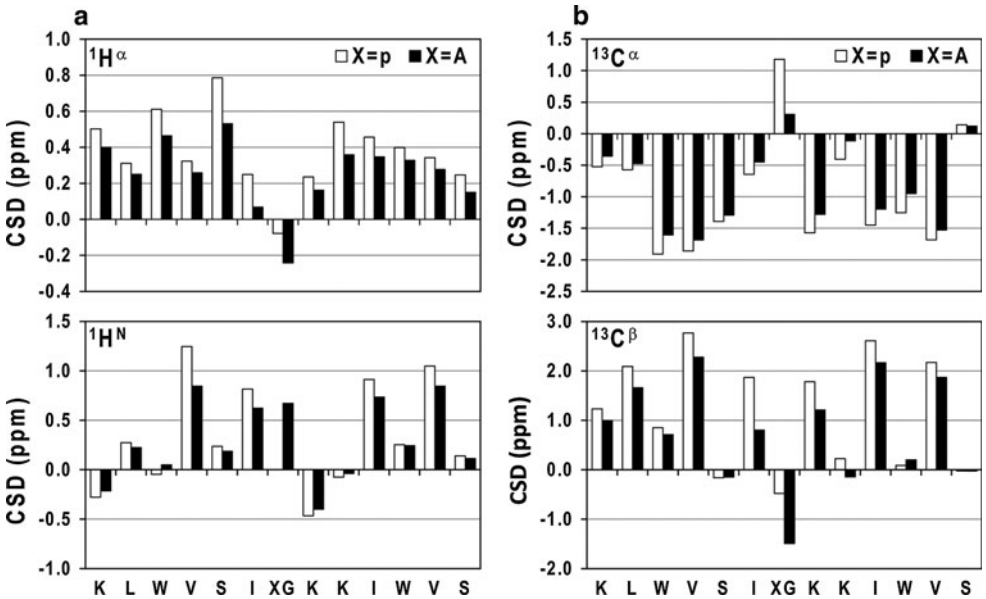

Fig. 5 **a** ^{1}H and **b** ^{13}C *CSD* histograms at 280 K for MrH4W4 scaffold containing pG (*open bars*) versus AG (*filled bars*) turn locus (XG). The entries for the XG turn locus are those of the X residue

rotamer preferences at H-bonded versus non-H-bonded sites do not appear to provide a rationale for the large differences in $^{13}C^{\beta}$ *CSD*s for these sites (vide infra).

Integrity of the $^{13}C^{\alpha/\beta}$ pattern in other β-sheet models

Four distinctly different classes of β-sheet models were examined to establish whether the alternating pattern of $^{13}C^{\alpha/\beta}$ *CSD*s is a general feature of antiparallel β-strand alignment, (1) a series of short hairpins with turn flanking aryl-aryl pairs, (2) an antiparallel β-construct held together by a disulfide linkage rather than a turn, (3) a series of β-capped hairpins of different length and turn types, and (4) a three-stranded sheet model. The peptide sequences are listed in Table 3 with the H-bonded sites underlined; β-capping residues, commencing with Trp's at a non-H-bonded site, are shown in blue. The data for the β-capped species will be presented first.

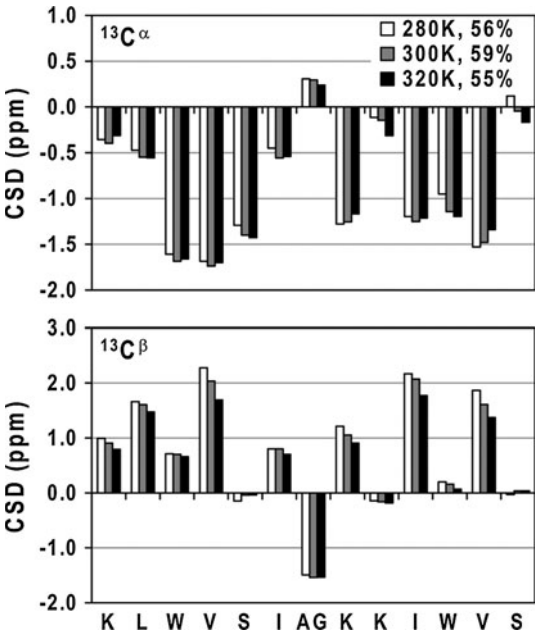

Fig. 6 MrH4W(±4)-AG $^{13}C^{\alpha/\beta}$ *CSD*s measured at 280, 300 and 320 K, the % fold measures from the $^{1}H^{\alpha}$ *CSD*s are also indicated

Table 3 Peptides for testing the generality of the $^{13}C^{\alpha/\beta}$ shift pattern in hairpins

Peptide	Sequence
βcap-INGK	Ac-W--INGK-WTG-NH_2
βcap-NPDGK	Ac-WVS-NPDGK-KIWTG-NH_2
βcap6-HG	Ac-WITVT--IHGK-KIRVWTG-NH_2
EPDGK-pG	Ac-VFIT-EPDGK-TYTE-VpGQ-KILQ-NH_2
turnless-C_2	C_2H_5-CO-WTT-VCI-RKWTGPK-NH_2
HP6Va3	KAVY-INGK-WTVE
HP7	KTW-NPATGK-WTE
HP7-AAA	KTW-NAAAGK-WTE
HP7(T→A)	KAW-NPATGK-WAE

Based on their cross-strand H-bonded status, the red underlined sites were expected to display the $^{13}C^{\alpha}$ downfield/$^{13}C^{\beta}$ upfield pattern; the black underlined positions are not as clearly of the H-bonded type

The β-cap hairpins have relatively immobilized termini when compared to non-capped isolated β-hairpins (Kier et al. 2010); as a result, the terminal residues adjacent to the capping motif, which have to be in register allowing the cross-strand hydrogen bonds to form, do not fray as much as is observed in many hairpins. If the alternating $^{13}C^{\alpha/\beta}$ shifts reflect the H-bonding status of strand sites, the pattern should be even clearer in these peptides, particularly at the turn remote strand sites. The ^{13}C *CSD* histograms (Fig. 7) reveal that this is the case: upfield $^{13}C^{\alpha}$ and downfield $^{13}C^{\beta}$ shifts are observed at the H-bonded sites and are more intense near the stabilizing β-cap.

The shifts appearing in the capping motif are also retained throughout the series, but are excluded from the present discussion; the TG residues do not have the ϕ/ψ torsional angles associated with β-strands.

In the βcap-INGK peptide, there is only a β-turn segment with a capping motif without strands. I2 and K5 are at *i* and i + 3 positions of the four-residue [2:2]-β-turn structure forming $NH_i \rightarrow C{=}O_{i+3}$ and $NH_{i+3} \rightarrow C{=}O_i$ hydrogen bonds, and the strong *CSD* shifts appear as expected, as well as for the IHGK [2:2] turn in the βcap6-HG peptide. In these species, the S ± 1 sites can be viewed as H-bonded strand sites. The fold populations and the specific H-bonds pattern have been confirmed by NH exchange protection studies (Kier and Andersen 2008; Kier et al. 2010).

NPDGK in βcap-NPDGK represents a [3:5]-(type I + Gly-bulge) turn conformation. The sequential pattern of $^{13}C^{\alpha/\beta}$ *CSD*s of the NPDGK turn region are in accord with the results of a statistical analyses of similar β-hairpins (Santiveri et al. 2001). Gly-bulge turns form $NH_i \rightarrow C{=}O_{i+4}$ and $NH_{i+3} \rightarrow C{=}O_i$ hydrogen bonds, but not $NH_{i+4} \rightarrow C{=}O_i$ bonds; however, the H-bonding within this loop does result in distinct $^{13}C^{\alpha/\beta}$ structuring shifts. The ^{13}C *CSD* characteristics of H-bonded strand sites likely reflects both H-bonding and the ϕ/ψ angles.

We have also used β-capping to design a very short β-sheet that lacks a reversing turn (Fig. S3); it provides yet another example of alternating $^{13}C^{\beta}$ *CSD* magnitudes with the H-bonded sites near the β-capping units displaying +3 ppm *CSD*s.

The three-stranded sheet system (EPDGK-pG), a double hairpin, presents complications not present in simple hairpins: (1) residues (T10–V14) in the second strand are all at positions where hydrogen bonds should form with both adjacent strands, which is not seen in an isolated β-hairpin; and (2) the effects of the N-terminal acetyl and C-terminal amide might not mimic those of extended strands, and (3) the peptide includes two aromatic residues which could change ^{13}C *CSD*s through ring current effects. In spite of that, the general traits of the ^{13}C *CSD* patterns summarized above can be still observed so long as: (1) we include ionization state changes in random coil values for the Glu sites, and (2) recognize that the EPDGK loop (like the NPDGK loop in the β-capped series) does not display the diagnostic shifts for the S ± 1 sites. Turn sites and β-strands can be recognized from the ^{13}C *CSD*s (Fig. 8). However, a number of the $^{13}C^{\beta}$ shifts are anomalous; these may be due to aromatic ring effects: for example, the central strand Tyr could influence neighboring shifts as well as those in both other strands. These effects are examined in the next section.

The last five entries in Table 3, including a β-sheet held together by a cystine rather than a turn, displayed $^{13}C^{\beta}$

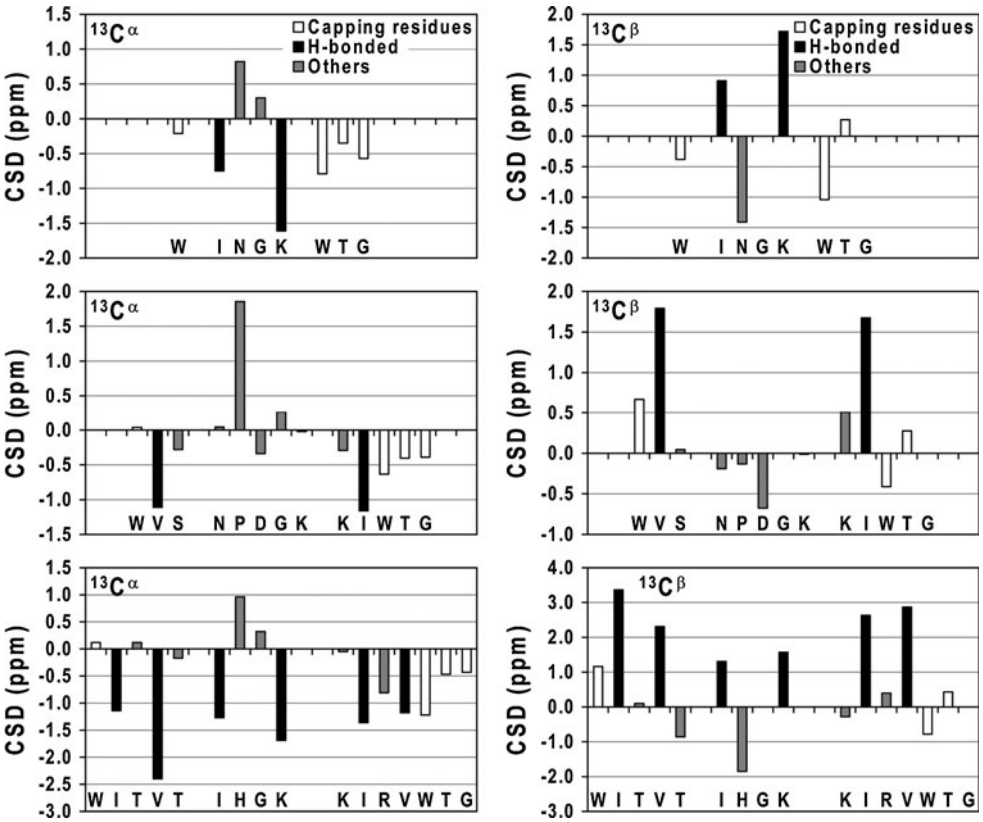

Fig. 7 $^{13}C^{\alpha}$ and $^{13}C^{\beta}$ *CSD* histograms of β-cap series at 280 K—the *CSD*s of the H-bonded S ± odd strand residues are in *black*, with β-capping motif in *white bars* and others in *light gray*, the S ± 1 sites in the NPDGK Gly-bulge loop do not follow the pattern observed for tight β-turns

CSD plots (see Fig. S3) that were fully consistent with the trends expected: the H-bonded sites highlighted by red underlining had $^{13}C^{\beta}$ *CSD*s of +2.36 ± 0.72 ppm, versus an average $^{13}C^{\beta}$ *CSD* of −0.02 (±0.6) ppm for the non-H-bonded sites. The HP7 series of peptides extends the observations to a [4:6]-hairpins, one of the first classes of protein hairpins that was shown to be stable outside of the protein context (Blanco et al. 1994; Kobayashi et al. 1993). The ^{13}C *CSD* histograms (Figs. S5 and S7) appear in the Supplementary Material.

Although the $^{13}C^{\alpha}$ *CSD*s at the H-bonded sites were all negative, the alternating H-bonded versus non-H-bonded pattern was not as clear in these species. Indeed, in the case of HP6Va3 (Fig. S2), the largest ^{13}C *CSD*s observed were unanticipated ones: N6-$^{13}C^{\alpha}$ (+4.1 ppm) and V11-$^{13}C^{\alpha}$ (−5.9 ppm). This prompted a more detailed consideration of ring current effects on ^{13}C shifts.

Hairpins containing aromatic residues and their $^{13}C^{\alpha/\beta}$ *CSD*s: ring current effects

As noted above, in hairpin HP6Va3 (Fig. S2) all of the $^{13}C^{\alpha/\beta}$ *CSD*s at the H-bonded sites displayed the expected sign. These and all other *CSD*s displayed melts that correspond to other spectroscopic measures of the warming-induced fold population decreases. Based on the NMR structure (Eidenschink et al. 2009b), the downfield (+2.6 ppm) shift at Y4-$^{13}C^{\alpha}$ and an upfield shift (−1.6 ppm) at Y3-$^{13}C^{\beta}$ could be attributed to the tyrosine ring and to shielding due to the face of the cross-strand W9 indole ring, respectively. The latter feature is observed at Trp-$^{13}C^{\beta}$ in the WTG cap of the β-cap peptides. The sign of the N6-$^{13}C^{\alpha}$ *CSD* is the same as that observed for other INGX turn species, but magnitude (+4.1 ppm) is at least twice that observed for any of the other systems examined (see Figs. 4b, 5b, 7). Initially, we thought that the very large upfield shift at V11-$^{13}C^{\alpha}$ (−5.9 ppm) might be attributed to the two negative charges of the E12 side chain as well as the free C-terminus; however the pH titration study of CRS-E (Ac-RKAEAGS) shows only downfield shifts at comparable sites upon ionization of the carboxylic acids. That leaves a ring current effect from W9 which is on the same face of the hairpin as a likely shift-perturbing candidate.

The MrH scaffold appeared to be better than HP6Va3 for probing ring current effects since its β-strand length provides multiple sites for the insertion of aromatic residues. A Trp/Trp pair was incorporated into the MrH4b construct at the S ± 2 (W2), S ± 3 (W3), and S ± 4 (W4) positions. The measured $^{1}H^{N}/^{1}H^{\alpha}$ *CSD*s (including comparisons to the same species in 20 % HFIP medium where fold populations exceed 95 % for all of the analogs) indicate that the Trp/Trp pairs at non-H-bonded sites increase the fold stability: MrH4b (48 % folded) to 80 and 70 % in

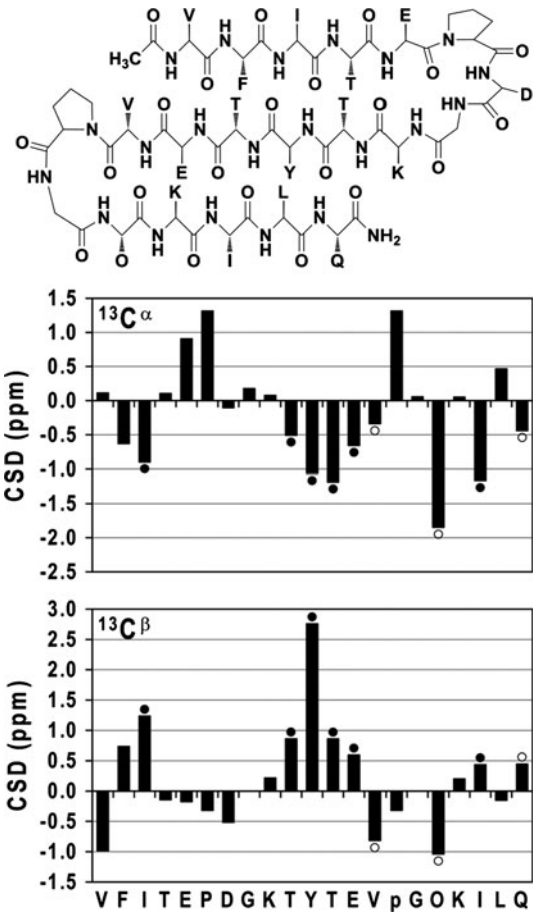

Fig. 8 Schematic view of three-stranded sheet EPDGK-pG and its $^{13}C^{\alpha}$ and $^{13}C^{\beta}$ *CSD* histograms at 280 K; the *circles* indicate the cross-strand hydrogen bonded sites of the peptide: the *solid* (*filled circle*) and the *open* (*empty circle*) *circles* correspond to the *red* and *black underlined* residues, respectively, in Table 3

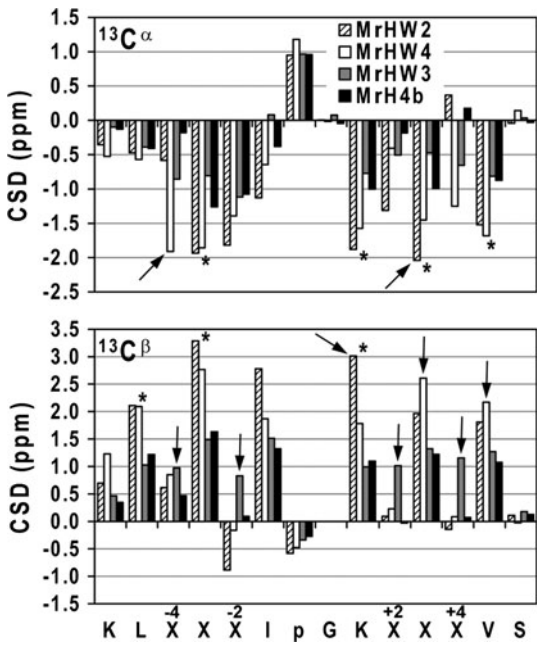

Fig. 9 *CSD*s at 280 K associated with the introduction of Trp/Trp pairs into the MrH4b scaffold. H-Bonded sites that echo the known changes in fold population are highlighted by *asterisk*. *Arrows* highlight *CSD*s influenced by ring current effects that are discussed in the text

MrH4bW2 and MrH4bW4 (Eidenschink et al. 2009b), respectively. With the H-bonded site placement of the Trp pair as in MrH4bW3 (Huggins and Andersen 2010) there is little change in fold stability; the complete *CSD* comparisons appear in Fig. S4. The key features, changes $^{13}C^{\alpha/\beta}$ *CSD* magnitudes, for discussing ring current effects appear in Fig. 9. At the H-bonded sites highlighted by asterisks, the $^{13}C^{\alpha/\beta}$ *CSD*s accurately mirror the fold populations. This is also the case for some non-H-bonded sites, but anomalies that can be attributed to ring current shifts are also observed.

The larger ring current effects are highlighted by arrows on Fig. 9. Reflecting the known and quite rigidly fixed EtF relationship of the indole rings of W6 and W11 in MrH4bW2, W6-$^{13}C^{\beta}$ is upfield by 0.9 ppm; this is nearly as large as the upfield shift observed for the farther upfield $^{1}H^{\beta}$ (−1.63 ppm) at this site: the entire methylene group experiences this cross-strand ring current effect. One general feature that can be recognized is downfield $^{13}C^{\beta}$ shifts at the sites immediately next to the inserted Trp's. There are clear instances of upfield shifts at $^{13}C^{\alpha}$ of the inserted Trp's (see Table S3). The balance of in-strand versus cross-strand ring current effects responsible for these are detailed in the Supplementary Material. The $^{13}C^{\beta}$ *CSD* histogram plot contains a number of examples in which the $^{13}C^{\beta}$ sites flanking the added W/W pair are further upfield than expected based on the secondary structure shift. This is most readily seen for MrH4bW3 (the positive $^{13}C^{\beta}$ *CSD*s at the S ± 2 and S ± 4 positions) in which the secondary structure shifts are smaller due to the lower fold population. The complete $^{13}C^{\alpha/\beta}$ plots also appear in Fig. S4. Even though there are ring current shifts that are comparable in magnitude to the diagnostic β-strand $^{13}C^{\alpha/\beta}$ structuring shifts, the strand register, alternating *CSD* magnitudes, can be observed in most cases, particularly for $^{13}C^{\beta}$. The only $^{13}C^{\beta}$ *CSD* histogram that was notably ambiguous was that of MrH4bW3, most readily seen in panel d) of Fig. S4, with the nearly constant $^{13}C^{\beta}$ *CSD*s along the strands reflect downfield ring current shifts at the S ± 2 and S ± 4.

The magnitude of $^{13}C^{\alpha/\beta}$ and $^{13}C'$ *CSD*s that represent 100 % folded values

With the exception of sites for which ring current shifts have been established, the $^{13}C^{\alpha/\beta}$ and $^{13}C'$ *CSD*s that were observed in all of the peptides in Table 1 were adjusted to

100 % folded values based on the extent of folding measured primarily by $^{1}H^{\alpha}$ *CSD*s of the non-hydrogen bonded residues. The averages and standard errors appear in Table 4.

In agreement with the ease with which strand periodicity could be recognized in *CSD* histograms, the $^{13}C^{\beta}$ *CSD*s at the H-bonded sites have the largest average *CSD* magnitudes. The *CSD*s at the non-H-bonded positions are zero, within experimental error. For $^{13}C'$ and $^{13}C^{\beta}$, there is no overlap between the shifts for H-bonded versus non-H-bonded strand sites. The (S − 1)-sites, for which H-bonding is less clear and involves an NH in the turn region in some case, displayed greater variability but retained β-strand rather than turn-like values. For turn sites, $^{13}C^{\alpha/\beta}$ *CSD*s display the opposite signs to those of the H-bonded strand sites. Although the standard errors are larger, the observation of a sign reversal for both $^{13}C^{\alpha}$ and $^{13}C^{\beta}$ *CSD*s at two or more adjacent sites identifies, with high probability, a turn locus in polypeptides.

Discussion

The examination of hairpin models was essential for the recognition of the ~1.1 ppm downfield shift associated with cross-strand H-bonded $^{1}H^{N}$ sites (versus non-H-bonded sites) in β-strands aligned antiparallel to another β-strand (Fesinmeyer et al. 2005a). Advocates of ^{13}C shifts for measuring hairpin fold populations (Santiveri et al. 2001, 2005), as well as chemical shift methods for assigning β versus α structure in proteins (Spera and Bax 1991; Wishart and Sykes 1994), have not distinguished between H-bonded and non-H-bonded sites. Also, given the general expectation (Iwadate et al. 1999; Santiveri et al. 2001) that ring current shifts and other diamagnetic anisotropy contributions to ^{13}C shifts should represent (relative to ^{1}H shifts) a smaller net contribution versus the secondary structure shifts, ^{13}C shifts should provide a better measure of secondary structure. In the present study, large differences in the *CSD*s of ^{13}C sites in H-bonded versus non-H-bonded sites are observed for all our β-sheet models. Excluding sites where ring current effects occur, and adjusting the observed shifts to "100 %-folded" values based fold population estimates from ^{1}H shifts and validated by NH exchange protection data (Kier and Andersen 2008; Kier et al. 2010) in many cases, the differences between H-bonded and non-H-bonded sites are greater than 1.2 ppm for all three ^{13}C probes examined (Table 4). This observation alone, prompts us to suggest that efforts to determine the extent of hairpin folding from ^{13}C shifts should be based exclusively on the observation for the cross-strand H-bonded sites. Furthermore, the statistics suggest the $^{13}C'$ and $^{13}C^{\beta}$ *CSD*s will provide the best differentiation with 100 %-folded *CSD* values approaching −2.6 and +3 ppm, respectively.

The present studies have shown that ^{13}C=O, $^{13}C^{\alpha}$ and $^{13}C^{\beta}$ of H-bonded strand residues in β-hairpins provide additional probes for quantitating the extent of folding. Even though aromatic residues inserted into hairpins may disrupt some diagnostic patterns and generate additional structuring shifts, it appears that all of the significant (>1 ppm) *CSD* magnitudes correlate with the extent of folding within a series of analogs. As a result, ^{13}C *CSD* melts provide an expansion of the probes available for assessing whether a two-state folding scenario is applicable for any particular fold. An additional ^{13}C shift melt supporting two-state behavior for the systems examined herein appears in Fig. S2. The melting analysis of $^{13}C^{\beta}$ sites, however, may need to be modified. In a number of ^{13}C *CSD* melts, including Figs. 6 and S2, the extent of structuring shift melting observed for the $^{13}C^{\beta}$ *CSD*s is somewhat greater than that seen for the $^{13}C^{\alpha}$ and backbone ^{1}H *CSD*s. This decrease in $^{13}C^{\beta}$ *CSD*s, corresponding to a *circa* 0.6 %/°C decrease in the fully folded *CSD*-value for $^{13}C^{\beta}$, that may reflect increased averaging of χ_1 on warming.

While the latter suggests that χ_1 can have some effect on the large $^{13}C^{\beta}$ *CSD*s at H-bonded sites in β-structures, a search through β-hairpin and β-sheet proteins failed to find large differences in rotamer preferences for H-bonded versus non-H-bonded sites and established that the differentiation of $^{13}C^{\beta}$ *CSD*s, between these sites can, for designed hairpins, be fully rationalized by variations in the backbone ϕ/ψ values (Shu et al. 2011). As a check on this, and to fully eliminate χ_1 as a significant contributor to $^{13}C^{\beta}$ *CSD*s in hairpins, we turned to alanine insertions. While the lower β-propensity of alanine often precludes placing it in the strands of β-hairpin designs, we were able to include peptides with Ala at both types of strand sites in the hairpin library used for this study. The strand alanines displayed

Table 4 Averaged 100 % *CSD* values at different sites in hairpins and other β-constructs

Sites for which there is an established ring current effect are excluded from the averages in this table

Site	HB	Non-HB strand	(S-1) in 4 and 6 residue loops	Turn sites (T1, T2, T3, T4)	
				All	Less Pro
^{13}C=O	−2.17 ± 0.51	+0.10 ± 0.52	nd	nd	nd
$^{13}C^{\alpha}$	−1.74 ± 0.76	−0.50 ± 0.84	−1.20 ± 0.68	+0.78 ± 1.27	+0.71 ± 1.44
$^{13}C^{\beta}$	+2.72 ± 0.78	+0.36 ± 0.56	+1.47 ± 1.01	−0.98 ± 1.46	−1.34 ± 1.65

$^{13}C'$ *CSD*s that are comparable to those of valine, including the dramatically enhanced values at the H-bonded sites (see Table S2).

This was extended to $^{13}C^{\alpha}$ and $^{13}C^{\beta}$ *CSD*s for several peptides (Figs. S6 and S7). The expected signs of the *CSD*s were observed for alanines at both types of sites. The positive $^{13}C^{\beta}$ *CSD*s at the H-bonded sites were as large as those observed for threonines. Thus, it appears that χ_1 preferences are not a major factor in the alternation of these *CSD*s along β-strands.

We believe the data presented herein make a strong case for using $^{13}C^{\alpha/\beta}$ and $^{13}C'$ *CSD*s comparisons over a series of hairpin analogs at a set temperature, preferably near 300 K, to assess relative fold stability. In addition $^{13}C'$ and $^{13}C^{\alpha}$ *CSD* melts can be used to monitor changes in the folding equilibrium constant with temperature. In the absence of 100 %-folded controls, $^{13}C'$ and $^{13}C^{\beta}$ *CSD* magnitudes can provide estimates of the folded population since there is relatively little variation in the 100 %-folded values observed: −2.6 for $^{13}C'$ and +3.0 ppm for $^{13}C^{\beta}$ are suggested as reasonable expectation values. The additional considerations required for doing this appear in the next section.

Reference shift selection, co-solvent and pH effect on ^{13}C shifts

The first requirement for the use of ^{13}C shifts as structural and melting probes is the availability of suitable statistical coil reference shifts and ascertaining whether these need to include near neighbor corrections or modifications due to co-solvent addition and/or pH changes. In the case of ^{13}C=O shifts, we continue to advocate (Shu et al. 2011) the use of local sequence matched ^{13}C=O isotopomer controls and the specific solvents employed in the hairpin peptide studies. In the absence of these, we recommend the Wishart coil values.

We evaluated three potential sources of $^{13}C^{\alpha/\beta}$ reference shifts (Fig. S1), and have settled on those of Wishart et al. (1995) as the best choice. The context differences, GGXGG for Schwartzinger versus GGXAGG and GGXPGG for Wishart, also appear to influence ^{13}C shifts. To illustrate this, we compared the Wishart coil shifts and the calculated shifts using the Schwartzinger method to the shifts observed for two of our unfolded controls (Ac-GKKITVSA and Ac-KAAVAA). The Wishart coil values are in much better agreement; e.g. for the Val site the observed $^{13}C^{\alpha/\beta}$ shifts were 0.16 ppm upfield ($^{13}C^{\alpha}$) and 0.21 ppm downfield ($^{13}C^{\beta}$) of the Wishart reference values. With the Schwartzinger method, the differences were −0.52 and +1.31 ppm. In absence of sequence-matched unfolded controls, the Wishart values appear to present the best reference set for $^{13}C^{\alpha/\beta}$ shifts.

The Wishart coil values were measured at pH 5, those of Schwartzinger at pH 2.3, as a result ionization-induced changes in coil shift values were expected for the C-terminal residue and for Glu and Asp residues. In general, carboxylic acid deprotonation results in downfield shifts. We measured the pH-induced shifts for our coil reference peptides. The adjustments can be as large as 2.8 ppm (for $^{13}C^{\beta}$ of Asp). The specific adjustments to the Wishart coil values that we now employ appear in the Methods section. In the absence of the C-terminal residue corrections, the C-terminal $^{13}C^{\alpha}$ displays rather large positive *CSD*s; Figs. S5, S6, S7, S8 provide examples.

Fluoroalcohols are often used in studies of β-sheet models. It has long been recognized that HFIP and TFE addition promote both α-helix and β-sheet formation. Even though the stabilizing mechanism is still unclear, it appears likely that upon fluoroalcohol addition there is a decrease in the H-bond accepting properties of the bulk solvent, which favors intramolecular H-bonding within the peptide and thus structuring (Andersen et al. 1996; Luo and Baldwin 1997; Buck 1998; Mehrnejad et al. 2007). Other factors that could influence chemical shifts are changes in dielectric constant and permittivity.

We found (see Table 2) that adding 8-20 % HFIP or 30 % TFE can not only influence the ^{13}C=O chemical shift (relative to DSS) of residues in random coil peptides but also that of urea. The shift changes for urea (+0.45 in 8 % HFIP, +1.05 in 20 % HFIP and −2.3 ppm in 30 % TFE) mirror those observed for the backbone ^{13}C=O of coil state peptides, suggesting similar interactions (notably H-bonding) with the modified bulk solvent. In contrast, the $^{13}C^{\alpha/\beta}$ coil reference shift changes are observed only for 30 % TFE and 20 % HFIP and are uniformly downfield. It was essential to correct (Fig. 4) for this effect to obtain $^{13}C^{\alpha/\beta}$ *CSD* magnitudes that correlated with the known fold population changes associated with fluoroalcohol addition.

As noted above, solvent effects on peptide fold formation are quite dramatic with HFIP and TFE addition increasing the stability of the hairpin fold; for example, in 30 vol% TFE even sequences with a normally turn-prohibiting L–Pro–Gly "turn locus" fold into the same hairpin motif as the Asn-Gly species. In the case MrH3d (KKYTVSI-PG-KKITVSA) the χ_F value is 0.52 in 30 vol% TFE at 280 K (Fesinmeyer et al. 2005a), based on backbone ^{1}H *CSD*s. MrH3d and the corresponding N-acetylated species were examined in the present study with $^{13}C'$ labels at the two H-bonded Val sites. Only with corrections for fluoroalcohol-containing media available, we were able to validate hairpin formation. The average $^{13}C'$ *CSD* of Ac-MrH3d was −0.05 ppm, in the absence of

added fluoroalcohol, increasing to −0.67 ppm in 30 vol% TFE (versus −0.95 ppm for the de-acetylated species, MrH3d). The $^{13}C'$ *CSD*s were well-correlated with the χ_F estimates from ^{1}H *CSD*s: Ac-MrH3d is only 33 % folded in 30 % TFE (versus 52 % for MrH3d). We attribute the decreased fold population upon acetylation to the removal of the favorable Coulombic interaction between the chain termini (Olsen et al. 2005).

Rationalizing the ^{13}C structuring shifts associated with hairpin formation

The most dramatic feature of our ^{13}C shift data for hairpins is the alternation of *CSD*s for non-H-bonded and H-bonded strand sites, with only the latter displaying the signs and large magnitudes that have been attributed to β-structure formation. In the case of H-bonded versus non-H-bonded ^{13}C=O sites, the sign of the *CSD* difference is the opposite of that expected for an intramolecular hydrogen bonding effect. In many systems, stronger H-bonding results in a downfield shift for the ^{13}C=O resonance (Case et al. 1994; Saito 1986). In Case's computational study of β-strand association effects (Xu and Case 2002), the cross-strand H-bonding effect was a downfield shift of circa 1 ppm. A similar deshielding effect was calculated for $^{13}C^{\alpha}$ sites. It would appear that these deshielding components are outweighed by other factors that differ between HB and non-HB sites in hairpins. An examination of NMR structures for eleven designed hairpins, including four examples included in the present chemical shift survey, has revealed a systematic alternation in ϕ/ψ values in β-strands as one move from HB to non-HB sites (Shu et al. 2011). These in ϕ/ψ value changes predicted the *CSD* magnitude changes we observed (Shu et al. 2011) and have confirmed herein. This raised the question of whether these same trends in both *CSD*s and ϕ/ψ values are observed in β-proteins.

Do hairpins and β-sheets in proteins display the patterns observed in designed models?

In extending our finds to proteins, we first examined three classes of proteins that contain relatively well-studied hairpins. The ϕ/ψ values seen in crystal structures are compared to those in designed hairpin in Fig. 10.

The protein hairpins display a muted version of the HB versus non-HB backbone torsion angle variation observed in designed hairpins. Related to this, we note that Santiveri et al. (2001) have examined the $^{13}C^{\alpha/\beta}$ shifts along 13 protein hairpins (including examples appearing in Fig. 10); the alternating-magnitude *CSD* patterns were much less obvious than in our hairpin model data.

To extend that study to a large body of β-proteins, we applied the procedures and definitions in the Methods section, to parse the ^{13}C chemical shifts that have been reported for proteins containing β-sheets and hairpins. The algorithm returns *CSD*s (based on Schwarzinger's *CSD* calculation method, the BMRB standard) and places them into three groups according to the residues' H-bonding

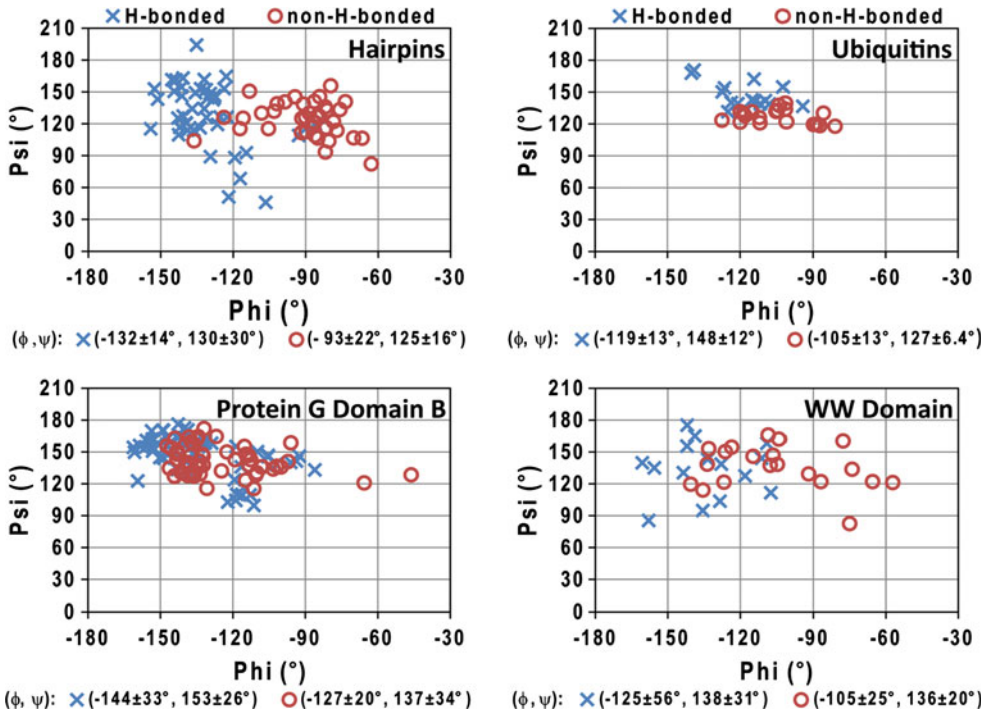

Fig. 10 Phi/Psi values for HB and non-HB sites in designed versus protein hairpins—the average values and standard error appear below each panel

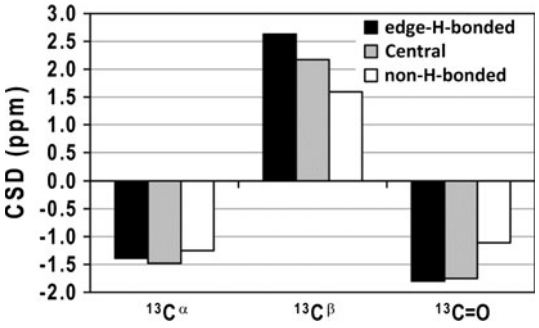

Fig. 11 Averaged ^{13}C *CSD*s for categorized residues in β-proteins

status: H-bonded (in an edge-strand), Central (with the amide unit H-bonded to two adjacent strands), and non-H-bonded. The results appear in Fig. 11.

The average *CSD* in the categories are fully consistent with those we observe in the hairpin models. The *CSD*s for the edge-strand H-bonded sites were larger and the differences between these and the non-H-bonded sites were in the same order, $^{13}C^{\beta} > {}^{13}C' > {}^{13}C^{\alpha}$, as was observed for the hairpins studied herein. Of some interest, the $^{13}C^{\beta}$ *CSD*s of H-bonded sites in edge-strands were larger than those for central sites, suggesting that the alternation of ϕ/ψ values observed in hairpins is muted or absent in central strands of larger β-sheets. The standard deviations of the mean values (ranging from 1.2 to 1.8 ppm), however, are larger than any of the differences.

We expect that a portion of the error is associated with the use of the Schwartzinger *CSD* protocol and the absence of sidechain ionization state adjustments to the Schwartzinger reference values that were obtained at pH 2.3. However, the more complicated contextual effects (diamagnetic anisotropy and electrostatic effects) in proteins, together with the relatively high probability of multiple aromatic groups in protein β-sheets may argue against using the alternating magnitude of $^{13}C^{\beta}$ *CSD*s along an edge β-strand as an analysis criterion for protein NMR data. One of the expected sources of error is confirmed by the data in Table 5.

We examined the HB versus non-HB *CSD*s derived using Schwartzinger's *CSD* protocol on a residue-specific level (Table 5). In the case of the more abundant $^{13}C^{\alpha}/^{13}C^{\beta}$ data, we included only the edge-strand H-bonded sites. From Table 5, it becomes clear that the lack of pH correction is, indeed a significant source of error. The more positive *CSD*s obtained for Glu and Asp (particularly for $^{13}C^{\beta}$) would be completely removed by using the Wishart coil values with the protonation state corrections given in the Methods section.

There are some other residues that give anomalous values in Table 5. The $^{13}C^{\alpha}$ *CSD*s for Asn and Thr (and Ser, −1.19 ppm for edge-H-bonded sites) are distinctly smaller than those for all other neutral amino acid residues. In the case of Thr (and Ser, data not shown) this extends to the $^{13}C^{\beta}$ *CSD*s as well. These likely represent H-bonding

Table 5 ^{13}C *CSD*s for H-bonded and non-H-bonded sites for selected residues

Residue	$^{13}C=O$		$^{13}C^{\alpha}$		$^{13}C^{\beta}$	
Type	HB	Non-HB	Edge-HB	Non-HB	Edge-HB	Non-HB
Arg	−1.61 (245)	−1.24 (100)	−1.66 (761)	−1.87 (473)	+2.19 (478)	+1.36 (311)
Asn	−1.57 (119)	−0.71 (57)	−0.64 (251)	−0.81 (207)	+2.20 (168)	+1.19 (141)
Asp	−0.44 (163)	+0.05 (57)	+1.11 (437)	+0.60 (237)	+4.69 (298)	+3.95 (182)
Gln	−1.69 (193)	−1.17 (79)	−1.52 (506)	−1.52 (352)	+2.10 (356)	+1.56 (224)
Glu	−1.16 (284)	−0.67 (169)	−0.94 (752)	−0.91 (752)	+2.77 (510)	+2.16 (548)
Lys	−1.86 (319)	−1.16 (151)	−1.61 (812)	−1.31 (521)	+1.97 (581)	+1.54 (378)
Phe	−1.82 (308)	−1.17 (127)	−1.73 (718)	−1.42 (438)	+1.81 (484)	+1.84 (312)
Thr	−1.71 (349)	−1.07 (243)	−0.63 (789)	−0.74 (895)	+0.84 (534)	+0.53 (629)
Val	−1.93 (666)	−1.20 (311)	−2.06 (1491)	−1.73 (1137)	+2.63 (1024)	+2.01 (786)
Averages						
For E,D	−0.90 (447)	−0.49 (226)	−0.18 (1189)	−0.55 (989)	+3.48 (808)	+2.61 (730)
Excluding anomalies[a]	−1.80[a] (2199)	−1.17[a] (1068)	−1.77[b] (5049)	−1.61[b] (3336)	+2.24[c] (5006)	+1.54[c] (3455)

The residue type is listed, and the number of such observations is indicated in parentheses below the average *CSD* for each type of ^{13}C sites in each residue

[a] For the carbonyl sites, only Glu and Asp (separately averaged) were excluded. All averages are frequency weighted

[b] In addition to Glu and Asp, the data for Asn and Thr were excluded from the overall average for the $^{13}C^{\alpha}$ *CSD*s; the data set for Ala (not shown) was added in

[c] In addition to Glu and Asp, the data for Thr were excluded from the overall average for the $^{13}C^{\alpha}$ *CSD*s; the data sets for Ala, Leu and Ile (not shown) were added in

(or hydration) effects in β-sheet geometries rather than the need for random coil shift adjustments.

Table 5 (and the variance in Fig. 11) has convinced us that better ^{13}C *CSD* calculation methods are needed in order to apply these shifts to detailed protein structure analysis. We are in the process of expanding our on-line CSDb program (Andersen et al. 1997; Eidenschink et al. 2009b; Fesinmeyer et al. 2004, http://andersenlab.chem.washington.edu/CSDb/) to include $^{13}C'$, $^{13}C^{\alpha}$, and $^{13}C^{\beta}$ with the coil values and corrections derived in the present and on-going studies.

Acknowledgments This work was supported by the National Science Foundation (grants CHE-0650318 and -1152218).

References

Andersen NH, Cort JR, Liu ZH, Sjoberg SJ, Tong H (1996) Cold denaturation of monomeric peptide helices. J Am Chem Soc 118:10309–10310

Andersen NH, Neidigh JW, Harris SM, Lee GM, Liu ZH, Tong H (1997) Extracting information from the temperature gradients of polypeptide NH chemical shifts. 1. The importance of conformational averaging. J Am Chem Soc 119:8547–8561

Andersen NH, Dyer RB, Fesinmeyer RM, Gai F, Liu ZH, Neidigh JW, Tong H (1999) Effect of hexafluoroisopropanol on the thermodynamics of peptide secondary structure formation. J Am Chem Soc 121:9879–9880

Andersen NH, Barua B, Fesinmeyer RM, Hudson FM, Lin JC, Euser A, White GW (2002) Chemical shifts, the ultimate test of peptide folding cooperativity. In: Benedetti E, Pedone C (eds) Proceedings of the 27th European peptide symposium, pp 824–825

Andersen NH, Fesinmeyer RM, Hudson FM (2004) Analysis of peptide β-sheet models using chemical shift deviations. In: Chorev M, Sawyer KT (eds) Peptide revolution: genetics, proteomics & therapeutics. Proceedings of the 18th American peptide symposium, pp 462–463

Andersen NH, Olsen KA, Fesinmeyer RM, Tan X, Hudson FM, Eidenschink LA, Farazi SR (2006) Minimization and optimization of designed β-hairpin folds. J Am Chem Soc 128:6101–6110

Avbelj F, Kocjan D, Baldwin RL (2004) Protein chemical shifts arising from α-helices and β-sheets depend on solvent exposure. Proc Natl Acad Sci U S A 101:17394–17397

Bax A, Davis DG (1985) MLEV-17-based two-dimensional homonuclear magnetization transfer spectroscopy. J Magn Reson 65:355–360

Blanco FJ, Rivas G, Serrano L (1994) A short linear peptide that folds into a native stable β-hairpin in aqueous solution. Nat Struct Biol 1:584–590

Buck M (1998) Trifluoroethanol and colleagues: cosolvents come of age. Recent studies with peptides and proteins. Q Rev Biophys 31:297–355

Case DA, Dyson HJ, Wright PE (1994) Use of chemical shifts and coupling constants in nuclear magnetic resonance structural studies on peptides and proteins. Methods Enzymol 239:392–416

de Dios AC, Oldfield E (1994) Chemical-shifts of carbonyl carbons in peptides and proteins. J Am Chem Soc 116:11485–11488

de Dios AC, Pearson JG, Oldfield E (1993) Secondary and tertiary structural effects on protein NMR chemical-shifts—an Ab initio approach. Science 260:1491–1496

Dyer RB, Maness SJ, Peterson ES, Franzen S, Fesinmeyer RM, Andersen NH (2004) The mechanism of β-hairpin formation. Biochemistry 43:11560–11566

Dyer RB, Maness SJ, Franzen S, Fesinmeyer RM, Olsen KA, Andersen NH (2005) Hairpin folding dynamics: the cold-denatured state is predisposed for rapid refolding. Biochemistry 44:10406–10415

Eidenschink L, Crabbe E, Andersen NH (2009a) Terminal side chain packing of a designed β-hairpin influences conformation and stability. Biopolymers 91:557–564

Eidenschink L, Kier BL, Huggins KN, Andersen NH (2009b) Very short peptides with stable folds: building on the interrelationship of Trp/Trp, Trp/cation, and Trp/backbone-amide interaction geometries. Proteins 75:308–322

Fesinmeyer RM, Hudson FM, Andersen NH (2004) Enhanced hairpin stability through loop design: the case of the protein G B1 domain hairpin. J Am Chem Soc 126:7238–7243

Fesinmeyer RM, Hudson FM, Olsen KA, White GW, Euser A, Andersen NH (2005a) Chemical shifts provide fold populations and register of β-hairpins and β-sheets. J Biomol NMR 33:213–231

Fesinmeyer RM, Peterson ES, Dyer RB, Andersen NH (2005b) Studies of helix fraying and solvation using 13C′ isotopomers. Protein Sci 14:2324–2332

Griffiths-Jones SR, Maynard AJ, Searle MS (1999) Dissecting the stability of a β-hairpin peptide that folds in water: NMR and molecular dynamics analysis of the β-turn and β-strand contributions to folding. J Mol Biol 292:1051–1069

Hudson FM, Andersen NH (2006) Measuring cooperativity in the formation of a three-stranded β-sheet (double hairpin). Biopolymers 83:424–433

Huggins KNL, Andersen NH (2010) Hairpin peptide inhibitors of amyloid fibrils formation. In: Lankinen H (eds) Chemistry of peptides in life science, technology and medicine. Proceedings of the 30th European peptide symposium, pp 590–591

Iwadate M, Asakura T, Williamson MP (1999) Cα and Cβ carbon-13 chemical shifts in proteins from an empirical database. J Biomol NMR 13:199–211

Kier BL, Andersen NH (2008) Probing the lower size limit for protein-like fold stability: ten-residue microproteins with specific, rigid structures in water. J Am Chem Soc 130:14675–14683

Kier BL, Andersen NH (2009) Short, hyperstable β-sheets without turns. Biopolym Peptide Sci 92:311

Kier BL, Shu I, Eidenschink LA, Andersen NH (2010) Stabilizing capping motif for beta-hairpins and sheets. Proc Natl Acad Sci U S A 107:10466–10471

Kobayashi N, Endo S, Munekata E (1993) Conformational study on the IgG binding domain of protein G. In: Peptide chemistry, pp 278–281

Luo P, Baldwin RL (1997) Mechanism of helix induction by trifluoroethanol: a framework for extrapolating the helix-forming properties of peptides from trifluoroethanol/water mixtures back to water. Biochemistry 36:8413–8421

Maynard AJ, Sharman GJ, Searle MS (1998) Origin of β-hairpin stability in solution: structural and thermodynamic analysis of the folding of model peptide supports hydrophobic stabilization in water. J Am Chem Soc 120:1996–2007

Mehrnejad F, Naderi-Manesh H, Ranjbar B (2007) The structural properties of magainin in water, TFE/water, and aqueous urea solutions: molecular dynamics simulations. Proteins 67:931–940

Olsen KA, Fesinmeyer RM, Stewart JM, Andersen NH (2005) Hairpin folding rates reflect mutations within and remote from the turn region. Proc Natl Acad Sci U S A 102:15483–15487

Piotto M, Saudek V, Sklenar V (1992) Gradient-tailored excitation for single-quantum NMR spectroscopy of aqueous solutions. J Biomol NMR 2:661–665

Saito H (1986) Conformation-dependent C-13 chemical-shifts—a new means of conformational characterization as obtained by high-resolution solid-state C-13 Nmr. Magn Reson Chem 24:835–852

Santiveri CM, Rico M, Jimenez MA (2001) 13C(alpha) and 13C(beta) chemical shifts as a tool to delineate beta-hairpin structures in peptides. J Biomol NMR 19:331–345

Santiveri CM, Pantoja-Uceda D, Rico M, Jimenez MA (2005) β-hairpin formation in aqueous solution and in the presence of trifluoroethanol: a (1)H and (13)C nuclear magnetic resonance conformational study of designed peptides. Biopolymers 79:150–162

Schenck HL, Gellman SH (1998) Use of a designed triple-stranded antiparallel β-sheet to probe β-sheet cooperativity in aqueous solution. J Am Chem Soc 120:4869–4870

Schwarzinger S, Kroon GJ, Foss TR, Wright PE, Dyson HJ (2000) Random coil chemical shifts in acidic 8 M urea: implementation of random coil shift data in NMRView. J Biomol NMR 18:43–48

Schwarzinger S, Kroon GJ, Foss TR, Chung J, Wright PE, Dyson HJ (2001) Sequence-dependent correction of random coil NMR chemical shifts. J Am Chem Soc 123:2970–2978

Sharman GJ, Griffiths-Jones SR, Jourdan M, Searle MS (2001) Effects of amino acid phi, psi propensities and secondary structure interactions in modulating Hα chemical shifts in peptide and protein β-sheet. J Am Chem Soc 123:12318–12324

Shu I, Stewart JM, Scian M, Kier BL, Andersen NH (2011) β-Sheet 13C structuring shifts appear only at the H-bonded sites of hairpins. J Am Chem Soc 133:1196–1199

Sibanda BL, Thornton JM (1991) Conformation of β-hairpins in protein structures: classification and diversity in homologous structures. Methods Enzymol 202:59–82

Spera S, Bax A (1991) Empirical correlation between protein backbone conformation and C-Alpha and C-Beta C-13 nuclear-magnetic-resonance chemical-shifts. J Am Chem Soc 113:5490–5492

Tatko CD, Waters ML (2003) The geometry and efficacy of cation-pi interactions in a diagonal position of a designed β-hairpin. Protein Sci 12:2443–2452

Vila JA, Scheraga HA (2008) Factors affecting the use of 13C(alpha) chemical shifts to determine, refine, and validate protein structures. Proteins 71:641–654

Vila JA, Arnautova YA, Scheraga HA (2008) Use of 13C(alpha) chemical shifts for accurate determination of β-sheet structures in solution. Proc Natl Acad Sci U S A 105:1891–1896

Vuister GW, Bax A (1992) Measurement of two-bond JCOH alpha coupling constants in proteins uniformly enriched with 13C. J Biomol NMR 2:401–405

Wishart DS, Sykes BD (1994) The 13C chemical-shift index: a simple method for the identification of protein secondary structure using 13C chemical-shift data. J Biomol NMR 4:171–180

Wishart DS, Sykes BD, Richards FM (1991) Relationship between nuclear magnetic resonance chemical shift and protein secondary structure. J Mol Biol 222:311–333

Wishart DS, Bigam CG, Holm A, Hodges RS, Sykes BD (1995) 1H, 13C and 15 N random coil NMR chemical shifts of the common amino acids. I. Investigations of nearest-neighbor effects. J Biomol NMR 5:67–81

Xu XP, Case DA (2002) Probing multiple effects on 15 N, 13C alpha, 13C beta, and 13C′ chemical shifts in peptides using density functional theory. Biopolymers 65:408–423